JSR Publications

Available Online

J. Sci. Res. **9** (4), 421-429 (2017)

JOURNAL OF SCIENTIFIC RESEARCH

www.banglajol.info/index.php/JSR

Studies on Adsorption Performance of Reactive Dye Remazol Navy RGB (RN-RGB) via Epoxide Functional Magnetic γ-Al_2O_3 Nanocomposite Particles

S. S. Bristy*, H. Ahmad

Department of Chemistry, Rajshahi University, Rajshahi 6205, Bangladesh

Received 31 May 2017, accepted in final revised form 16 October 2017

Abstract

The nanocomposite particles named as γ-Al_2O_3/Fe_3O_4/SiO_2/poly(glycidyl methacrylate) or γ-Al_2O_3/Fe_3O_4/SiO_2/PGMA were prepared by multi-step process. At first, γ- Al_2O_3 nanoparticles were prepared by sol-gel method. Magnetite, Fe_3O_4, nanoparticles were then precipitated by in situ co-precipitation in presence of γ-Al_2O_3 particles, followed by incorporation of mesoporous silica layer using Stöber process. Finally, the surface of the γ-Al_2O_3/Fe_3O_4/SiO_2 nanocomposite particles was modified by seeded polymerization of GMA using free radical polymerization. The surface modification, morphology and size distribution of the prepared nanocomposite particles were confirmed by FTIR, scanning electron microscopy (SEM) and thermogravimetric analysis (TGA). The adsorption capacity of γ-Al_2O_3/Fe_3O_4/SiO_2/PGMA nanocomposite particles was evaluated using remazol navy RGB (RN-RGB) as a model dye.

Keywords: γ- Al_2O_3; PGMA; Seeded polymerization; Remazol navy RGB; Adsorption.

doi: http://dx.doi.org/10.3329/jsr.v9i4.32729 J. Sci. Res. **9** (4), 421-429 (2017)

1. Introduction

Porous ceramics have become increasingly important in industry due to their numerous applications and utilizations [1]. Alumina (Al_2O_3) is used for making porous ceramics because most of the alumina-based ceramics possess relatively high strength along with improved thermal and chemical stability [2]. Porous Al_2O_3 materials are used in various forms e.g. as polymeric foams for packaging and porous ceramics for water purification [3]. Among different classes of Al_2O_3 the crystal structure of γ-Al_2O_3 is of hexagonal plate with large surface area. This made the γ-Al_2O_3 useful in catalysis and in absorbent applications [4]. Within the last 15 years, inorganic nanostructures including metal oxides, ceramics and composites have gained more and more attraction to the scientific world and

* *Corresponding author:* ssb10ru@gmail.com

stimulated research on sometimes fancy ideas for future applications like molecular manufacturing or space elevators as well as on serious products for consumer goods, health, medical or food technology [5-9]. Nanomaterials provide a powerful tool for detection and treatment of pollutants from the environment. Among the varieties of the superparamagnetic nanoparticles Fe_3O_4 has received extensive attentions due to its unique magnetic properties and feasibility of preparation [10-12], high surface to volume ratio. In this study, we focused on Fe_3O_4 - γ-Al_2O_3 mixed nanocomposite. The combination of multiple materials often minimizes or masks the adverse properties of individual component materials to yield a better result. Combining the above two kinds of materials (porous ceramic γ-Al_2O_3 and Fe_3O_4) it is possible to develop new ceramic-nanoceramic composites which could be used as adsorbents and magnetic supports of high effectiveness because of their ability to be prepared in granular and other engineered form.

In the present investigation attempt was made to prepare hybrid epoxide functional γ-Al_2O_3/Fe_3O_4/SiO_2/poly(glycidyl methacrylate) or γ-Al_2O_3/Fe_3O_4/SiO_2/PGMA nanocomposite polymer particles via seeded polymerization in presence of γ-Al_2O_3/Fe_3O_4/SiO_2 nanocomposite seed particles. SiO_2 layer is incorporated on γ-Al_2O_3/Fe_3O_4 nanocomposite particles to make the surface compatible for seeded polymerization [13]. These hybrid magnetic polymer particles are capable to ensure a strong magnetic response and polymeric material can provide favorable functional groups and ability to protect nanoparticles aggregation [14]. The adsorptive potential of γ-Al_2O_3/Fe_3O_4/SiO_2/PGMA nanocomposite particles was evaluated for removal of remazol navy RGB (RN-RGB), an azo dye used extensively in the commercial textile industry.

2.1. *Materials*

Aluminium nitrate nonahydrate $Al(NO_3)_3.9H_2O$ and urea both from E-Merck, Germany, cationic surfactant cetyl trimethyl ammonium bromide (CTAB) from Fluka, Biochemica, Switzerland were used without purification. Tetraethyl orthosilicate (TEOS) from Sigma-Aldrich Chemie, USA, was preserved in refrigerator before use. Glycidyl methacrylate (GMA) of monomer grade purchased from Fluka, Chemika, Switzerland was passed through activated basic alumina column to remove inhibitors. 2,2'-Azobis(2-amidinopropane)dihydrochloride (V-50) from LOBA Chem. India, was recrystallized from distilled water and preserved in the refrigerator before use. RN-RGB was obtained from a local dye industry. Ferric chloride ($FeCl_3$), ferrous sulphate heptahydrate ($FeSO_4.7H_2O$), NH_4OH, citric acid, HNO_3 acid and other chemicals were of analytical grade.

Scanning electron microscope or SEM (Hitachi, SU8000, Japan) was used to see the morphology and particle size distribution. IR spectrophotometer, FTIR (Perkin Elmer, FTIR-100, UK) was used for surface analysis. Thermal analyses were carried out using thermal analyzer, TGA (STA 8000, Perkin Elmer, Netherlands). Visible Spectrophotometer (Optima SP-300, Tokyo, Japan) was used during adsorption experiment of dye. Centrifuge machine (TG16-WS) from Kokuson Corporation, Tokyo,

Japan was used for separating the dye loaded nonocomposite particles after dye adsorption.

2.2. *Preparation of γ-Al_2O_3 particles*

$Al(NO_3)_3.9H_2O$ (35 g), distilled deionized water (35 g) and urea (72 g) were mixed keeping the molar ratio of Al^{3+}/urea at 1/13 and magnetically stirred at ~200 rpm for about 1 h. Temperature was then raised to 90°C and heating was continued for around 12 h to yield Al_2O_3 sol. The sol was heated for another 3 h to a transparent gel. The freshly prepared Al_2O_3 gel was dried at 300°C for 3 h to eliminate the remaining urea and nitrate.

2.3. *Preparation of γ-Al_2O_3/Fe_3O_4 nanocomposite particles*

At first, 0.0125 g cationic surfactant (CTAB) was added to washed γ-Al_2O_3 particles (0.5 g) dispersed in 10 g water. The mixture was added to water (51.50 g) and cooled to 0-5°C in an ice bath. Fe_3O_4 nanoparticles were prepared by co-precipitation of Fe^{2+} and Fe^{3+} from their aqueous alkaline solutions (molar ratio 1:1.87). For this purpose, $FeSO_4{\cdot}7H_2O$ (0.3753 g) and $FeCl_3$ (0.4380 g) were dissolved in water in presence of TRAB stabilized γ-Al_2O_3 dispersion under nitrogen gas bubbling. The reaction mixture in a two necked round flask was transferred to a preheated oil bath at 85°C. After 30 min, 25% NH_4OH (8.0 g) solution was added to the mixture and stirred for 2 h. The prepared γ-Al_2O_3/Fe_3O_4 dispersion was treated with HNO_3 (2M) (1.30 g) for 15 min and washed magnetically with water until the solution was neutral. Then 0.4 M citric acid solution (5.60 g) was added slowly and stirred overnight to stabilize the prepared nanocomposite particles. Citrate stabilized γ-Al_2O_3/Fe_3O_4 nanocomposite particles were repeatedly washed by deionized distilled water to remove excess citric acid.

2.4. *Preparation of γ-Al_2O_3/Fe_3O_4/SiO_2 nanocomposite particles*

Deionized water (2.0 g), EtOH (4.09 g), and CTAB powder (0.196 g) were mixed and stirred at 60°C for complete dissolution of CTAB. The citrate stabilized γ-Al_2O_3/Fe_3O_4 nanocomposite particles (0.5 g) dispersed in water (24.75 g) was added to the mixture. After 30 min 25% NH_4OH solution (0.26 g) and TEOS (0.5 g) were added dropwise. The mixture was stirred at 60°C for 2 h to obtain γ-Al_2O_3/ Fe_3O_4/SiO_2 nanocomposite particles.

2.5. *Preparation of γ-Al_2O_3/Fe_3O_4/SiO_2/PGMA nanocomposite particles*

γ-Al_2O_3/Fe_3O_4/SiO_2 nanocomposite particles (0.2 g) dispersed in water (17 g) was taken in a three necked round bottomed flask dipped in a thermostat water bath maintained at 75°C. GMA (0.40 g) was added into the reaction flask and polymerization was started using initiator V-50 (0.012 g). The mixture was stirred mechanically at 100 rpm for 12 h under a nitrogen gas. The produced nanocomposite particles were washed magnetically

three times by deionised distilled water to remove any unreacted monomer and initiator fragments.

2.6. *Adsorption procedure*

Continuous adsorption experiments were carried out in 100 mL beakers containing the dye solution of the desired concentration and the known amount of γ-Al_2O_3/Fe_3O_4/SiO_2/PGMA nanocomposite particles. The beaker was covered with aluminium foil and magnetically stirred till equilibrium time was reached. The dye solution was then separated from the adsorbent by centrifugation at 1200 rpm and the remaining dye concentration in the supernatant was determined by using visible spectrophotometer at its specific λ_{max} (620 nm).

Dye uptake at equilibrium q_e was determined by,
$q_e = (C_0 - C_e)\ V/W$

Where C_0 and C_e (mg/L) are the initial and equilibrium concentrations of the dye solutions, V (L) is the volume of the solution and W (g) is the mass of the adsorbent used.

Also percentage of removal (%R) of dye was calculated from
$\%\ R = [(C_0 - C_e)/C_0] \times 100$
Continuous experiments were performed at different time intervals and different initial dye concentrations.

3. Results and Discussion

Fig. 1A represents FT-IR spectra of Fe_3O_4 nanoparticles, γ-Al_2O_3 particles, γ-Al_2O_3/Fe_3O_4 and γ-Al_2O_3/Fe_3O_4/SiO_2 nanocomposite particles. In the spectrum of Fe_3O_4 nanoparticles, characteristic stretching vibrations due to Fe-O bonds appeared at 398 and 583 cm^{-1} respectively. In the spectrum of γ-Al_2O_3 particles the absorption bands appeared at ~521.34 and ~797 cm^{-1} represent aluminium ions (Al^{3+}) in octahedral and tetrahedral environments respectively [15]. Broad O-H stretching band appeared at around 3444 cm^{-1} revealed the presence of hydroxyl groups. In the FT-IR spectrum of citrate stabilized γ-Al_2O_3/Fe_3O_4 nanocomposite the absorption peaks of Al–O bond in the range of 400-800 cm^{-1} cannot be identified due to their superimpose on the absorption peaks of Fe-O bond in the same region. A weak absorption band at ~1735 cm^{-1} corresponds to C=O bond is derived from citric acid. In the FT-IR spectrum of as-synthesized γ-Al_2O_3/Fe_3O_4/SiO_2 nanocomposite particles presence of additional Si-O-Si asymmetric and symmetric stretching vibration bands at ~1027.82 and 799 cm^{-1} respectively imply the successful encapsulation of γ-Al_2O_3/Fe_3O_4 nanocomposite particles by SiO_2 layer. Comparatively, the spectrum of γ-Al_2O_3/Fe_3O_4/SiO_2/PGMA nanocomposite polymer particles (Fig. 1B)

shows new strong absorption signals at 1729.10 and 1153.40 cm^{-1} due to characteristic C=O and C-O stretching vibration of ester group derived from GMA monomers.

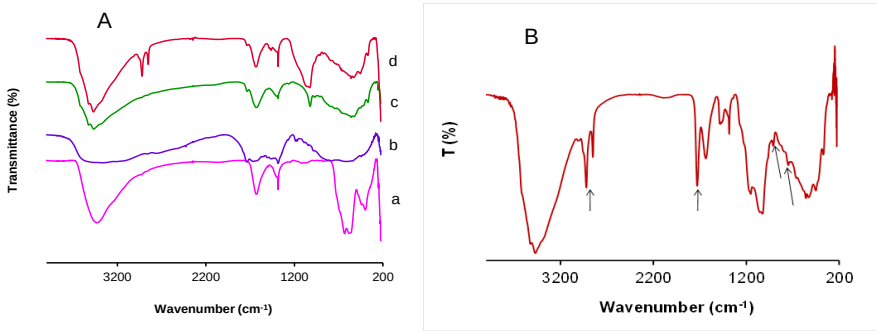

Fig. 1. A) FT-IR spectra of a) Fe_3O_4 nanoparticles, b) γ-Al_2O_3 particles, c) γ-Al_2O_3/Fe_3O_4 and d) γ-Al_2O_3/Fe_3O_4/SiO_2 nanocomposite particles. B) FTIR spectrum of γ-Al_2O_3/Fe_3O_4/SiO_2/PGMA nanocomposite particles.

TGA thermogram of γ-Al_2O_3 particles illustrated in Fig. 2a shows two major mass loss regions. The initial mass loss occurs until ~136°C is due to the evaporation of physisorbed water and the second mass loss appears at 280°C is due to dehydroxylation (caused by the breaking of Al-OH bonds). In TGA thermogram of γ-Al_2O_3/Fe_3O_4 nanocomposite (Fig. 2b) mass loss reduces slightly due to the increase in inorganic content though the composite particles are modified with citric acid. The incorporation of silica layer in γ-Al_2O_3/Fe_3O_4 nanocomposite increases the mass loss by 0.78% although the overall inorganic content increases. This increase in mass loss is probably due to breaking of Si-OH bond in silica at higher temperature. Compared to γ-Al_2O_3/Fe_3O_4/SiO_2 nanocomposite particles, further modification by PGMA increases the mass loss by 14.66%. This mass loss behavior confirms the formation of γ-Al_2O_3/Fe_3O_4/SiO_2/PGMA composite particles containing ~ 14% PGMA.

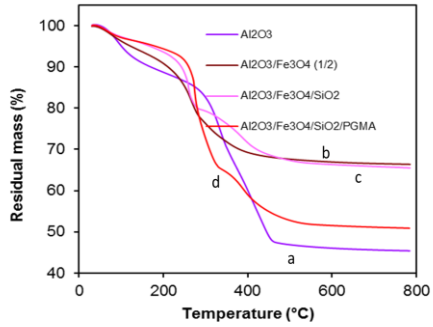

Fig. 2. TGA thermograms of a) γ-Al_2O_3 particles, b) γ-Al_2O_3/Fe_3O_4, c) γ-Al_2O_3/ Fe_3O_4/SiO_2 and d) γ-Al_2O_3/Fe_3O_4/SiO_2/PGMA nanocomposite particles.

From the SEM image of γ-Al_2O_3 particles (Fig. 3) some hexagonal flake shaped particles can be observed. Following precipitation of magnetic iron oxide on the surface of γ-Al_2O_3 particles**,** the morphology of γ-Al_2O_3/Fe_3O_4 nanocomposite particles bit changed to some needle like morphology. Such orientation may have occurred either during preparation or during drying for SEM sample preparation as rarely observed for magnetic particles [16]. The morphology of γ-Al_2O_3/Fe_3O_4/SiO_2 nanocomposite particles is mostly spherical and the needle like orientation of γ-Al_2O_3/Fe_3O_4 composite particles almost disappears, possibly owing to the weakened magnetic interaction resulted from the coverage with silica layer. In the SEM image (Fig. 3d) of γ-Al_2O_3/Fe_3O_4/SiO_2/PGMA nanocomposite particles cluster type morphology could be observed.

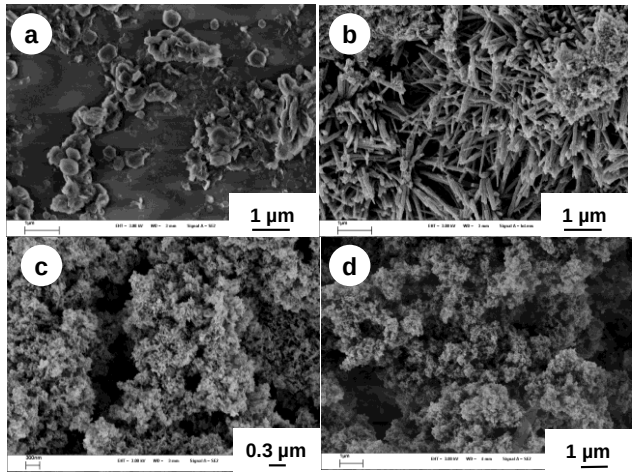

Fig. 3. SEM images of a) γ-Al_2O_3 particles b) γ-Al_2O_3/Fe_3O_4, c) γ-Al_2O_3/Fe_3O_4/SiO_2 and d) γ-Al_2O_3/Fe_3O_4/SiO_2/PGMA nanocmposite particles.

The contact time dependent change in removal efficiency of RN-RGB by γ-Al_2O_3/Fe_3O_4/SiO_2/PGMA nanocomposite particles (0.01 g) with initial dye concentration being adjusted to 100 mg/L is shown in Fig. 4. The mechanism of dye removal can be described by the migration of the dye molecule from the solution to the adsorbent particle and diffusion through the surface [17]. It can be noticed that initially dye adsorption is rapid and thereafter, the adsorption magnitude remained unchanged. At this point, the amount of dye being adsorbed onto the adsorbent was in a state of dynamic equilibrium with the amount of dye desorbed from the adsorbent [18]. The time required to attain this state of equilibrium was taken as the equilibrium time and the amount of dye removed at the equilibrium time reflected the maximum dye adsorption capacity of the adsorbent under the experiment conditions [19].

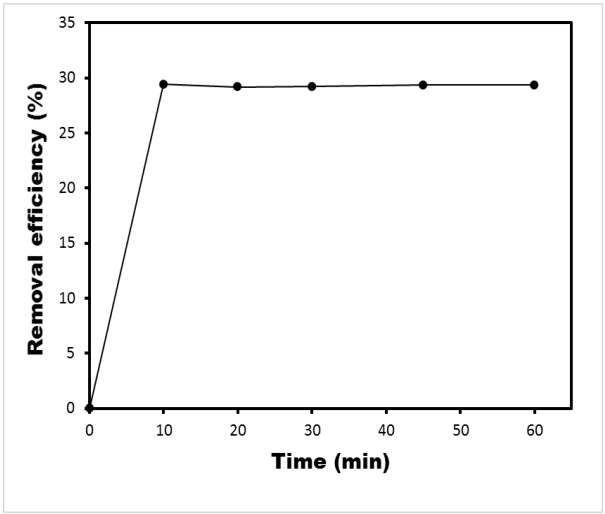

Fig. 4. Effect of contact time on the removal of RN-RGB dye by γ-Al_2O_3/Fe_3O_4/SiO_2/PGMA nanocomposite particles. Dye concentration 100 mg/L, Particle 0.01 g, Total volume 30 mL, Temperature 30°C, pH 7.45.

The effect of initial dye concentration on percentage adsorption of the dye is shown in Fig. 5A. The adsorption of the dye at equilibrium decreases from 92.45% to 29.40% with increase in dye concentration from 20 mg/L to 100 mg/L (Fig. 5a). This may be attributed to surplus dye molecules being present in the solution, with respect to the available active adsorption sites owing to fixed surface area of γ-Al_2O_3/Fe_3O_4/SiO_2/PGMA nanocomposite particles [20]. As shown in Fig. 5B, the adsorption magnitude on γ-Al_2O_3/Fe_3O_4/SiO_2/PGMA nanocomposite particles increases with the increase in the initial dye concentration. Initial concentration provides an important driving force to overcome all mass transfer resistance of the reactive dye between the aqueous and solid phases [21].

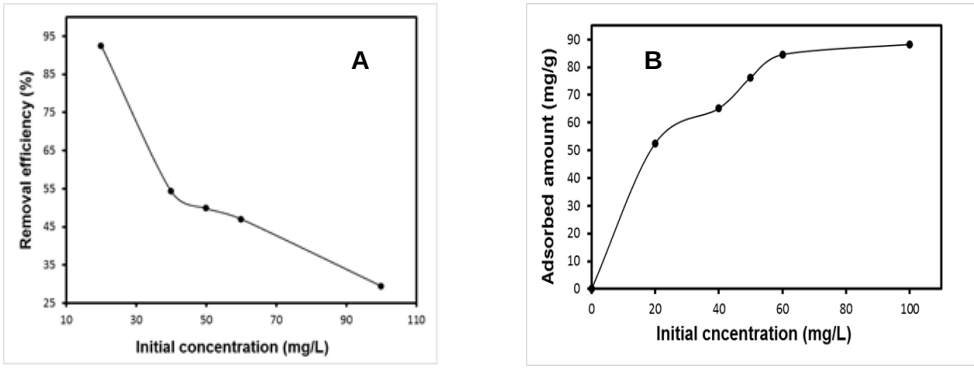

Fig. 5. Effect of initial dye concentration on the (A, B) adsorption behavior of RN-RGB on γ-Al_2O_3/Fe_3O_4/SiO_2/PGMA nanocomposite particles. Particle 0.01 g, Total volume 30 mL, Temperature 30°C, pH 7.45, Time 10 min.

4. Conclusion

Epoxide functional magnetic γ-Al_2O_3/Fe_3O_4/SiO_2/PGMA nanocomposite particles were prepared following a four steps process. At first, γ-Al_2O_3 particles were synthesized followed by in situ precipitation of Fe_3O_4 particles to prepare γ-Al_2O_3/Fe_3O_4 nanocomposite particles. The resulted γ-Al_2O_3/Fe_3O_4 particles were encapsulated by SiO_2 layer. Finally, the synthesized γ-Al_2O_3/Fe_3O_4/SiO_2 nanocomposite particles were functionalized by PGMA. All the synthesized particles were confirmed from their detailed characterization by FT-IR spectra, TGA thermograms and SEM images. The adsorption performance of reactive dye RN-RGB via γ-Al_2O_3/Fe_3O_4/SiO_2/PGMA nanocomposite particles was studied. It was observed that the prepared nanocomposite particles can be used as effective adsorbent for adsorptive removal of organic pollutant from waste water.

Acknowledgment

Authors are thankful to Central Science Laboratory, Rajshahi University, Rajshahi, Dr. Klaus Tauer, MPI of Colloid & Interfaces, Germany, Dr. Hideto Minami, Associate Professor, Graduate School of Science and Technology, Kobe University, Japan, for instrumental support.

References

1. M. J. Ribeiro, J. C. Abrantes, J. M. Ferreira, and J. A. Labrincha, Ceram. Int. **28**, 319 (2002). https://doi.org/10.1016/S0272-8842(01)00097-9
2. J. F. Poco, J. H. Satcher Jr, and L. W. Hrubesh, J. Non Cryst. Solids **285**, 57 (2001). https://doi.org/10.1016/S0022-3093(01)00432-X
3. R. W. Rice, Porosity of Ceramics (Marcel Dekker Inc. New York, 1998).
4. L. Samain, A. Jaworski, M. Edén, D. M. Ladd, D.-K. Seo, F. J. Garcia- Garcia, and U. Häussermann, J. Solid State Chem. **217**, 1 (2014). https://doi.org/10.1016/j.jssc.2014.05.004
5. M. Krummenacker and J. Lewis, Prospects in Nanotechnology toward Molecular Manufacturing (John Wiley & Sons, New York, USA, 1995).
6. B. Bhushan, Springer Handbook of Nanotechnology (Springer, Germany, 2004).
7. NASA Science, Science News: Audacious & Outrageous: Space elevators, http://science.nasa.gov/headlines/y2000/ast07sep_1.htm (accessed December 2009).
8. W. Luther and G. Bachmann, Nanoparticles-Small Thing, Big Effects; German Federal Ministry of Education and Research, Division Nanomaterials, New Materials (2008).
9. J. H. Fendler, Nanoparticles and Nanostructured Films: Preparation, Characterization and Applications (Wiley-VCH, Germany, 1998). https://doi.org/10.1002/9783527612079
10. R. Shabnam and H. Ahmad, Polym. Adv. Technol. **26**, 408 (2015). https://doi.org/10.1002/pat.3468
11. H. Ahmad, M. Nurunnabi, M. M. Rahman, K. Kumar, K. Tauer, H. Minami, and M. A. Gafur, Colloid Surfaces A: Physicochem. Eng. Aspects **459**, 39 (2014). https://doi.org/10.1016/j.colsurfa.2014.06.038
12. H. Ahmad, K. Kumar, M. M. Rahman, M. A. J. Miah, H. Minami, and MA. Nuri, Polym. Adv. Technol. **24**,740 (2013). https://doi.org/10.1002/pat.3138
13. H. Gleiter, Soid State, Mater. Sci. **6**, 205 (2002).
14. X. Wang, Z. Zhou, and G. Jing, Bioresource Technol. **130**, 750 (2013). https://doi.org/10.1016/j.biortech.2012.12.010

15. M. R. Karim, M. A. Rahman, M. A. Miah, H. Ahmad, M. Yanagiswa, and M. Ito, Open Colloid Sci. J. **4**, 32 (2011).
16. P. Poddar, T. Telem-Shafir, T. Fried, and G. Markovich, Phys. Rev. B **66**, 060403 (2002). https://doi.org/10.1103/PhysRevB.66.060403
17. S. Banerjee, R. K. Gautam, A. Jaiswal, M. C. Chattopadhyaya, and Y. C. Sharma, RSC Adv. **5**, 14425 (2015).
18. R. Ansari and Z. Mosayebzadeh, J. Iran Chem. Soc. **7**, 339 (2010). https://doi.org/10.1007/BF03246019
19. M. A. Ahmad and N. K. Rahman, Chem. Eng. J. **170**, 154 (2011). https://doi.org/10.1016/j.cej.2011.03.045
20. G. M. Ratnamala, K. Vidya Shetty, and G. Srinikethan, Water, Air Soil Pollut. **223**, 6187 (2012). https://doi.org/10.1007/s11270-012-1349-4
21. M. H. Karaoglu, M. Dogan, and M. Alkan, Desalination **256**, 154 (2010). https://doi.org/10.1016/j.desal.2010.01.021